Pramana – J. Phys. (2017) 89:65
DOI 10.1007/s12043-017-1466-0

Right-handed currents at $B \to K^*\ell^+\ell^-$ kinematic endpoint

RUSA MANDAL[1], ANIRBAN KARAN[1], ABINASH KUMAR NAYAK[1], RAHUL SINHA[1,*] and TOM BROWDER[2]

[1]The Institute of Mathematical Sciences, HBNI, Taramani, Chennai 600 113, India
[2]Department of Physics and Astronomy, University of Hawaii, Honolulu, HI 96822, USA
*Corresponding author. E-mail: sinha@imsc.res.in

Published online 9 October 2017

Abstract. The rare decay $B \to K^*\ell^+\ell^-$ is a very significant mode to search for physics beyond the Standard Model (SM). The mode provides a very rich spectrum of observables obtained from the angular distribution of its decay products. The recent LHCb measured values of these observables are used to conclude an evidence of right-handed currents at the kinematic endpoint of this decay mode. As the conclusion is drawn at the maximum dilepton invariant mass square (q^2) kinematic endpoint, it relies only on heavy quark symmetries where it is valid without significant corrections.

Keywords. New Physics; right-handed currents.

PACS Nos 11.30.Er; 13.25.Hw; 12.60.−i

1. Introduction

The decay $B \to K^*\ell^+\ell^-$ is a $b \to s$ flavour changing neutral current (FCNC) process that occurs through loops in the Standard Model (SM). Hence, it provides an indirect but sensitive probe for physics beyond SM or New Physics (NP). The large number of observables, obtained from its angular distributions, can be used to get around the hadronic uncertainties which usually hinder any effort to make precise theoretical estimates. Various experts have devoted significant attention [1–8] to probe NP through this particular mode. Most of the previous works have focussed on the low dilepton invariant mass squared region $q^2 = 1$–6 GeV^2, while only a few have considered the large q^2 region.

We shall be particularly interested in the maximum q^2 region, which will show a very clean probe for NP. Using the recent LHCb measured values of these observables, we find a clear evidence of the right-handed currents, along with possibilities for some particular kind of other NP contributions. The conclusions are drawn at the $q^2_{\rm max}$ kinematic endpoint of this decay mode, using heavy quark symmetries where it is valid without significant corrections. As the heavy quark symmetries are very reliable at $q^2_{\rm max}$, our conclusions are free from hadronic uncertainties. With the kind of NP we are analysing, the observable values are unaltered from their SM values at $q^2_{\rm max}$. However, their derivatives get significant contributions from these kinds of NP. In this approach, we look for NP in these derivatives of the observables using the given experimental data.

2. Theoretical framework

In SM, for the massless lepton limit, the decay $B \to K^*\ell^+\ell^-$ is described by the following six transversity amplitudes [8]:

$$\mathcal{A}_\lambda^{\rm L,R} = C^\lambda_{\rm L,R}\,\mathcal{F}_\lambda - \tilde{\mathcal{G}}_\lambda = (\tilde{C}_9^\lambda \mp C_{10})\mathcal{F}_\lambda - \tilde{\mathcal{G}}_\lambda, \qquad (1)$$

where λ runs over three polarizations, i.e. perpendicular ($\perp$), parallel ($\parallel$) and longitudinal (0). This parametric form of the observables is a very generic form and well established in the literature. This form incorporates all the short-distance effects, long-distance effects, factorizable contributions, non-factorizable contributions and all order electromagnetic corrections to the hadronic operators, into the theory.

C_9 and C_{10} in eq. (1) are Wilson coefficients whereas $\tilde{C}_9^\lambda$ is the redefined 'effective' Wilson coefficient expressed [8–10] as

$$\tilde{C}_9^\lambda = C_9 + \Delta C_9^{\rm (fac)}(q^2) + \Delta C_9^{\lambda,{\rm (non\text{-}fac)}}(q^2), \qquad (2)$$

where $\Delta C_9^{\rm (fac)}(q^2)$ and $\Delta C_9^{\lambda,{\rm (non\text{-}fac)}}(q^2)$ denote factorizable and non-factorizable contributions. However, C_{10}

does not get any contribution through strong interaction effects coming from electromagnetic corrections to hadronic operators [11]. The form factors $\mathcal{F}_\lambda$ and $\tilde{\mathcal{G}}_\lambda$ in eq. (1) are related to the conventional form factors of the decay mode, as shown in the appendix of ref. [8].

The imaginary contributions to the SM amplitudes, coming through $\tilde{C}_9^\lambda$ and $\tilde{\mathcal{G}}_\lambda$, are taken into account. $\mathcal{F}_\lambda$'s and C_{10} are real in SM. We define two variables r_λ, ε_λ and rewrite the amplitudes $\mathcal{A}_\lambda^{\mathrm{L,R}}$ in eq. (1) as

$$\mathcal{A}_\lambda^{\mathrm{L,R}} = (\mp C_{10} - r_\lambda)\mathcal{F}_\lambda + i\varepsilon_\lambda, \tag{3}$$

where

$$r_\lambda = \frac{\mathrm{Re}(\tilde{\mathcal{G}}_\lambda)}{\mathcal{F}_\lambda} - \mathrm{Re}(\tilde{C}_9^\lambda), \tag{4}$$

$$\varepsilon_\lambda = \mathrm{Im}(\tilde{C}_9^\lambda)\mathcal{F}_\lambda - \mathrm{Im}(\tilde{\mathcal{G}}_\lambda). \tag{5}$$

The observables $F_\perp$, $F_\parallel$, F_L, A_FB and A_5 are given as

$$F_\lambda = \frac{|\mathcal{A}_\lambda^\mathrm{L}|^2 + |\mathcal{A}_\lambda^\mathrm{R}|^2}{\Gamma_f}, \quad \lambda \in \{\perp, \parallel, 0\}, \tag{6}$$

$$A_\mathrm{FB} = \frac{3}{2}\frac{\mathrm{Re}(\mathcal{A}_\parallel^\mathrm{L}\mathcal{A}_\perp^{\mathrm{L}*} - \mathcal{A}_\parallel^\mathrm{R}\mathcal{A}_\perp^{\mathrm{R}*})}{\Gamma_f}, \tag{7}$$

$$A_5 = \frac{3}{2\sqrt{2}}\frac{\mathrm{Re}(\mathcal{A}_0^\mathrm{L}\mathcal{A}_\perp^{\mathrm{L}*} - \mathcal{A}_0^\mathrm{R}\mathcal{A}_\perp^{\mathrm{R}*})}{\Gamma_f}, \tag{8}$$

with $\Gamma_f \equiv \sum_\lambda(|\mathcal{A}_\lambda^\mathrm{L}|^2 + |\mathcal{A}_\lambda^\mathrm{R}|^2)$.

On the other hand, with the inclusion of the RH currents, the transversity amplitudes are expressed as [11]

$$\mathcal{A}_\perp^{\mathrm{L,R}} = \big((\tilde{C}_9^\perp + C_9') \mp (C_{10} + C_{10}')\big)\mathcal{F}_\perp - \tilde{\mathcal{G}}_\perp \tag{9}$$

$$\mathcal{A}_\parallel^{\mathrm{L,R}} = \big((\tilde{C}_9^\parallel - C_9') \mp (C_{10} - C_{10}')\big)\mathcal{F}_\parallel - \tilde{\mathcal{G}}_\parallel \tag{10}$$

$$\mathcal{A}_0^{\mathrm{L,R}} = \big((\tilde{C}_9^0 - C_9') \mp (C_{10} - C_{10}')\big)\mathcal{F}_0 - \tilde{\mathcal{G}}_0. \tag{11}$$

As expected, we get back our SM amplitudes defined in eq. (1) when we set C_9' and C_{10}', the RH contributions to the amplitudes, to zero. Note that in defining transversity amplitudes for RH counterparts, we have ignored the imaginary contributions. This is done just for convenience. We do take into account the imaginary contributions in this analysis. However, for notational ease, we do not explicitly mention ε_λ in our equations.

We define two new variables, ξ and ξ', by taking ratios of the RH and SM Wilson coefficients, i.e.

$$\xi = \frac{C_{10}'}{C_{10}} \quad \text{and} \quad \xi' = \frac{C_9'}{C_{10}}\,. \tag{12}$$

With these new variables, the observables $F_\perp$, $F_\parallel$, A_FB, A_5 (eqs (6)–(8)) are casted in the following form:

$$F_\perp = 2\zeta(1+\xi)^2(1+R_\perp^2), \tag{13}$$

$$F_\parallel \mathsf{P}_1^2 = 2\zeta(1-\xi)^2(1+R_\parallel^2), \tag{14}$$

$$F_\mathrm{L}\mathsf{P}_2^2 = 2\zeta(1-\xi)^2(1+R_0^2), \tag{15}$$

$$A_\mathrm{FB}\mathsf{P}_1 = 3\zeta(1-\xi^2)(R_\parallel + R_\perp), \tag{16}$$

$$\sqrt{2}A_5\mathsf{P}_2 = 3\zeta(1-\xi^2)(R_0 + R_\perp), \tag{17}$$

where

$$\mathsf{P}_1 = \frac{\mathcal{F}_\perp}{\mathcal{F}_\parallel}, \quad \mathsf{P}_2 = \frac{\mathcal{F}_\perp}{\mathcal{F}_0}, \quad \zeta = \frac{\mathcal{F}_\perp^2 C_{10}^2}{\Gamma_f},$$
$$R_\perp = \frac{(r_\perp/C_{10}) - \xi'}{1+\xi}, \quad R_\parallel = \frac{(r_\parallel/C_{10}) + \xi'}{1-\xi},$$
$$R_0 = \frac{(r_0/C_{10}) + \xi'}{1-\xi}. \tag{18}$$

Our main objective is to solve for the theoretical parameters in terms of the experimentally observable quantities. However, we have one parameter as compared to the number of independent observables. From eqs (13)–(17) and the constraint $F_\mathrm{L} + F_\parallel + F_\perp = 1$, $R_\perp$, $R_\parallel$, R_0 and P_2 can be expressed in terms of the observables and P_1:

$$R_\perp = \pm\frac{3}{2}\frac{((1-\xi)/(1+\xi))F_\perp + \frac{1}{2}\mathsf{P}_1 Z_1}{\mathsf{P}_1 A_\mathrm{FB}} \tag{19}$$

$$R_\parallel = \pm\frac{3}{2}\frac{((1+\xi)/(1-\xi))\mathsf{P}_1 F_\parallel + \frac{1}{2}Z_1}{A_\mathrm{FB}} \tag{20}$$

$$R_0 = \pm\frac{3}{2\sqrt{2}}\frac{((1+\xi)/(1-\xi))\mathsf{P}_2 F_\mathrm{L} + \frac{1}{2}Z_2}{A_5} \tag{21}$$

$$\mathsf{P}_2 = \frac{((1-\xi)/(1+\xi))2\mathsf{P}_1 A_\mathrm{FB} F_\perp}{\sqrt{2}A_5\,(((1-\xi)/(1+\xi))2F_\perp + Z_1\mathsf{P}_1) - Z_2\mathsf{P}_1 A_\mathrm{FB}} \tag{22}$$

with

$$Z_1 = \left(4F_\parallel F_\perp - \frac{16}{9}A_\mathrm{FB}^2\right)^{1/2} \tag{23}$$

and

$$Z_2 = \left(4F_\mathrm{L}F_\perp - \frac{32}{9}A_5^2\right)^{1/2}. \tag{24}$$

Hence, we look for additional relations among the parameters which can be used to overcome this difficulty. Fortunately, at q^2_max, the heavy quark symmetries provide a relation among the form factors which can be used to eliminate the remaining one parameter.

2.1 *Constraints at* q^2_max

At the maximum q^2 kinematic endpoint (q^2_max), the amplitudes are constrained from both the kinematics and the heavy quark symmetries. These constraints, which give the observables very unique values at this endpoint, and the values of the observables are given in refs [6–8],

where the values of the observables are given as

$$F_{\rm L}(q^2_{\rm max}) = \frac{1}{3}, \quad F_{\parallel}(q^2_{\rm max}) = \frac{2}{3}, \quad A_4(q^2_{\rm max}) = \frac{2}{3\pi},$$
$$F_{\perp}(q^2_{\rm max}) = 0, \quad A_{\rm FB}(q^2_{\rm max}) = 0, \quad A_{5,7,8,9}(q^2_{\rm max}) = 0. \tag{25}$$

Even in the presence of right-handed currents, these values remain unaltered.

2.2 *The limit $q^2 \to q^2_{\rm max}$*

Though the RH currents do not effect the values of the observables at $q^2_{\rm max}$, they have substantial effect on the behaviour of the observables just away from the endpoint. Hence, we put our efforts in studying this region, i.e. $q^2 \to q^2_{\rm max}$.

In [3,12], the authors study the large q^2 region where K^* has low recoil energy. There it is shown that in this $q^2_{\rm max}$ limit, the hadronic form factors obey certain conditions, i.e.

$$\frac{\tilde{\mathcal{G}}_{\parallel}}{\mathcal{F}_{\parallel}} = \frac{\tilde{\mathcal{G}}_{\perp}}{\mathcal{F}_{\perp}} = \frac{\tilde{\mathcal{G}}_0}{\mathcal{F}_0} = -\kappa \frac{2 m_b m_B C_7}{q^2}. \tag{26}$$

Here $\kappa \approx 1$ [12]. As seen from eq. (4), eq. (26) implies that $r_0 = r_{\parallel} = r_{\perp} \equiv r$ [13] at $q^2_{\rm max}$ in SM. As eq. (26) holds equally good even in the presence of RH currents in the theory, from eq. (18) we can easily see that $R_0 = R_{\parallel} \neq R_{\perp}$ at $q^2 = q^2_{\rm max}$. At this point we insist that, at $q^2_{\rm max}$, the non-factorizable and resonance contributions do not affect this relation [6]. Hence, the presence of right-handed currents can be inferred by just measuring these R_λs.

2.3 *Observable expansions around $q^2_{\rm max}$*

R_λ values are studied around $q^2_{\rm max}$. From eq. (13) we have $F_{\perp}(q^2_{\rm max}) = 0$ which implies $\zeta = 0$ in the limit $q^2 \to q^2_{\rm max}$. We also have $R_{\parallel}(q^2_{\rm max}) = R_0(q^2_{\rm max})$ which along with eqs (14) and (15) imply $\mathsf{P}_2 = \sqrt{2}\,\mathsf{P}_1$ at $q^2_{\rm max}$. But, both P_1 and P_2 vanish at $q^2_{\rm max}$. However, their ratio survives. Also the observables have fixed values at $q^2_{\rm max}$.

As we want to analyse R_λ in the limit $q^2 \to q^2_{\rm max}$, i.e. away from the endpoint, we Taylor expand the transversity amplitudes around $q^2_{\rm max}$ in terms of $\delta \equiv q^2_{\rm max} - q^2$. However, the expansion should account for the relative momentum dependence of the transversity amplitudes $\mathcal{A}^{\rm L,R}_\lambda$, e.g. according to eqs (6)–(8) and (25) the perpendicular polarized amplitudes ($\mathcal{A}^{\rm L,R}_\perp$) must have $\mathcal{O}(\sqrt{\delta})$ higher-order expansion than the other polarization amplitudes ($\mathcal{A}^{\rm L,R}_{\parallel,0}$). This has also been shown in ref. [6]. This distinction between the expansions of different polarization amplitudes should also reflect in the corresponding expansion of the observables.

Taking all these into consideration, we finally expand the observables as follows:

$$F_{\rm L} = \frac{1}{3} + F_{\rm L}^{(1)}\delta + F_{\rm L}^{(2)}\delta^2 + F_{\rm L}^{(3)}\delta^3 \tag{27}$$

$$F_{\perp} = F_{\perp}^{(1)}\delta + F_{\perp}^{(2)}\delta^2 + F_{\perp}^{(3)}\delta^3 \tag{28}$$

$$A_{\rm FB} = A_{\rm FB}^{(1)}\delta^{1/2} + A_{\rm FB}^{(2)}\delta^{3/2} + A_{\rm FB}^{(3)}\delta^{5/2} \tag{29}$$

$$A_5 = A_5^{(1)}\delta^{1/2} + A_5^{(2)}\delta^{3/2} + A_5^{(3)}\delta^{5/2}. \tag{30}$$

Here, $O^{(n)}$ is the coefficient of the nth term in the expansion of the observable O. The limiting values of the observables are easily seen to be satisfying in the above form of expansions.

However, these polynomial expansions cannot account for the q^2-dependent behaviour of the resonances which are ever present in the experimental data. So it is imperative to study the effect of resonances on our analysis. The systematics of these resonances are analysed in length in ref. [7] which strengthen our claims.

2.4 *R_λ expressions*

We now try to express R_λs in terms of the observable coefficients O^n. We start with eq. (26) between form factors which is expected to hold for $q^2 \to q^2_{\rm max}$. For eq. (26) to hold for the mentioned limit, it should satisfy the following relation up to all orders in the expansion:

$$q^2 \frac{\tilde{\mathcal{G}}_\lambda}{\mathcal{F}_\lambda} = q^2_{\rm max} \frac{\tilde{\mathcal{G}}_\lambda^{(1)} + \delta(\tilde{\mathcal{G}}_\lambda^{(2)} - (\tilde{\mathcal{G}}_\lambda^{(1)}/q^2_{\rm max})) + \mathcal{O}(\delta^2)}{\mathcal{F}_\lambda^{(1)} + \delta\,\mathcal{F}_\lambda^{(2)} + \mathcal{O}(\delta^2)}. \tag{31}$$

However, we only assume that this relation is valid up to order δ. If eq. (31) were to have a constant value around $q^2_{\rm max}$ up to $\mathcal{O}(\delta)$, then we must have $\mathcal{F}_\lambda^{(2)} = c\,\mathcal{F}_\lambda^{(1)}$ and $(q^2_{\rm max}\,\tilde{\mathcal{G}}_\lambda^{(2)} - \tilde{\mathcal{G}}_\lambda^{(1)}) = c\,q^2_{\rm max}\,\tilde{\mathcal{G}}_\lambda^{(1)}$ where c is any constant. We already have $\mathsf{P}_2 = \sqrt{2}\mathsf{P}_1$ at $q^2_{\rm max}$, which means we must have $\mathsf{P}_2^{(1)} = \sqrt{2}\mathsf{P}_1^{(1)}$, where $\mathsf{P}_{1,2}^{(1)}$ are the coefficients of the leading $\mathcal{O}(\sqrt{\delta})$ terms in the expansions of $\mathsf{P}_{1,2}$. This, along with $\mathcal{F}_\lambda^{(2)} = c\,\mathcal{F}_\lambda^{(1)}$, implies $\mathsf{P}_2^{(2)} = \sqrt{2}\mathsf{P}_1^{(2)}$. This is the needed input which along with eq. (22) expresses $\mathsf{P}_1^{(1)}$ purely in terms of observable coefficients.

With this assumption, we find the expressions for R_λ in the limit $q^2 \to q^2_{\rm max}$ as follows:

Table 1. The best-fit and 1σ errors of the coefficients of observables (in eqs (27)–(30)) obtained by fitting the observables, as a function of q^2, to the recent LHCb's 14-bin measurements [14] for the entire q^2 region.

	$O^{(1)}$ (10^{-2})	$O^{(2)}$ (10^{-3})	$O^{(3)}$ (10^{-4})
$F_{\rm L}$	-2.94 ± 1.36	12.27 ± 2.05	-5.73 ± 0.72
$F_{\perp}$	6.83 ± 1.75	-9.67 ± 2.59	3.77 ± 0.90
$A_{\rm FB}$	-30.59 ± 2.37	26.75 ± 4.42	-4.00 ± 1.83
A_5	-16.57 ± 2.36	6.77 ± 4.18	1.94 ± 1.61

$$R_{\perp}(q^2_{\rm max}) = \frac{8A^{(1)}_{\rm FB}(-2A^{(2)}_5 + A^{(2)}_{\rm FB}) + 9(3F^{(1)}_{\rm L} + F^{(1)}_{\perp})F^{(1)}_{\perp}}{8(2A^{(2)}_5 - A^{(2)}_{\rm FB})\sqrt{\frac{3}{2}F^{(1)}_{\perp} - A^{(1)\,2}_{\rm FB}}} = \frac{\omega_2 - \omega_1}{\omega_2\sqrt{\omega_1 - 1}}, \tag{32}$$

$$R_{\parallel}(q^2_{\rm max}) = \frac{3(3F^{(1)}_{\rm L} + F^{(1)}_{\perp})\sqrt{\frac{3}{2}F^{(1)}_{\perp} - A^{(1)\,2}_{\rm FB}}}{-8A^{(2)}_5 + 4A^{(1)}_{\rm FB} + 3A^{(1)}_{\rm FB}(3F^{(1)}_{\rm L} + F^{(1)}_{\perp})} = \frac{\sqrt{\omega_1 - 1}}{\omega_2 - 1} = R_0(q^2_{\rm max}), \tag{33}$$

where

$$\omega_1 = \frac{3}{2}\frac{F^{(1)}_{\perp}}{A^{(1)\,2}_{\rm FB}} \quad \text{and} \quad \omega_2 = \frac{4(2A^{(2)}_5 - A^{(2)}_{\rm FB})}{3A^{(1)}_{\rm FB}(3F^{(1)}_{\rm L} + F^{(1)}_{\perp})}. \tag{34}$$

As we see from these expressions, even at the endpoint, R_λ depends on polynomial coefficients $F^{(1)}_{\rm L}$, $F^{(1)}_{\perp}$, $A^{(2)}_{\rm FB}$ and $A^{(2)}_5$ which are not related by HQET. So, corrections beyond HQET are automatically incorporated through fitting of data in our approach.

3. Data analysis

If RH currents or other NP that treat the '$\perp$' amplitude differently are not present, one would expect $R_{\perp}(q^2_{\rm max}) = R_{\parallel}(q^2_{\rm max}) = R_0(q^2_{\rm max})$. As RH currents are not seen elsewhere, we cannot expect their contribution to be very large. For restricting ξ and ξ' to reasonably small values, we must have $R_{\perp} \neq R_{\parallel} = R_0$ and $R_\lambda > 0$. This condition can be shown easily as the LHS of eq. (16) is positive around $q^2_{\rm max}$ and $\zeta > 0$.

3.1 *Polynomial fitting of the observables*

We fit the latest LHCb measurements [14] of the observables $F_{\rm L}$, $F_{\perp}$, $A_{\rm FB}$ and A_5 as functions of q^2 using Taylor expansion at $q^2_{\rm max}$. This fitting is not related to heavy quark effective theory (HQET) or any other theoretical assumption. At first, we define χ^2 function by comparing bin-integrated values of the parametric form of the observables with their experimentally measured values for all 14 bins. It should be noted that the bin integrations are done taking q^2 function of observables weighted with recent measurements of differential decay rate [15]. Then, minimizing the χ^2 function, we obtain analytic fits for different observables. To get better constraints near the endpoint, we used 14 bin data set from LHCb, based on the method of moments [16] instead of 8 bin data set. We have varied the order of polynomials fitted as different observables and the number of bins used in fitting (from last four to fourteen). It is observed that the fits show good convergence if the order of the polynomials lies within 2 to 4 and larger numbers of bins are taken into account. The systematics of polynomial fitting is described in detail in ref. [7]. The best-fit values for each coefficient of the observables $F_{\rm L}$, $F_{\perp}$, $A_{\rm FB}$ and A_5 (eqs (27)–(30)) are given in table 1. The errors in each coefficient are evaluated using a covariance matrix technique (figures 2 and 3).

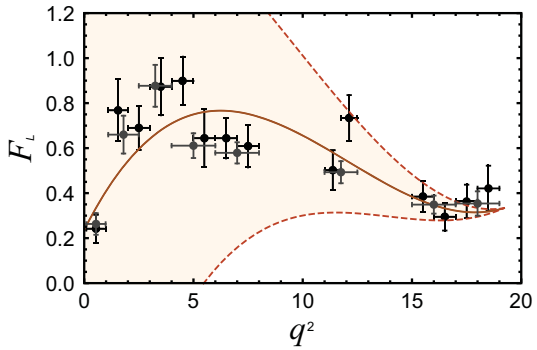

Figure 1. An analytic fit to 14-bin LHCb data using Taylor expansion around $q^2_{\rm max}$ for the helicity fraction $F_{\rm L}$ is demonstrated. The central fit function is shown as the brown curve. The light brown shaded regions denote the $\pm 1\sigma$ error bands. The LHCb 14-bin and 8-bin measurements [14] are indicated by the points with the black and gray error bars, respectively.

The best fits for the observables $F_{\rm L}$, $F_{\perp}$, $A_{\rm FB}$ and A_5 along with their error bands and LHCb measured data are presented in figures 1–4. As we have neglected the correlation between different observables, we treat

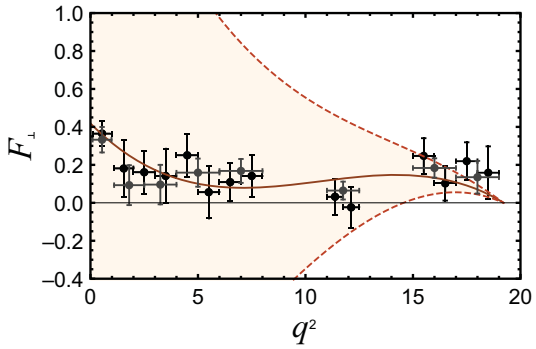

Figure 2. An analytic fit to 14-bin LHCb data using Taylor expansion around $q^2_{\rm max}$ for the helicity fraction $F_\perp$ is demonstrated. The central fit function is shown as the brown curve. The light brown shaded regions denote the $\pm 1\sigma$ error bands. The LHCb 14-bin and 8-bin measurements [14] are indicated by the points with the black and gray error bars, respectively.

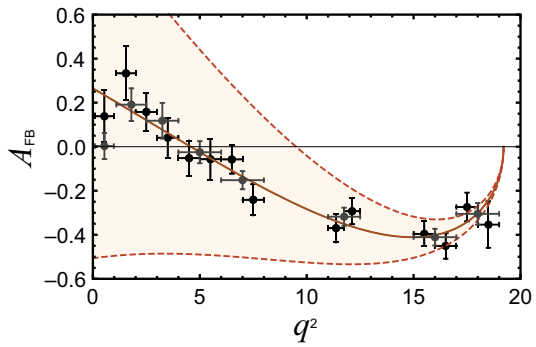

Figure 3. An analytic fit to 14-bin LHCb data using Taylor expansion around $q^2_{\rm max}$ for the asymmetry $A_{\rm FB}$ is demonstrated. The central fit function is shown as the brown curve. The light brown shaded regions denote the $\pm 1\sigma$ error bands. The LHCb 14-bin and 8-bin measurements [14] are indicated by the points with the black and gray error bars, respectively.

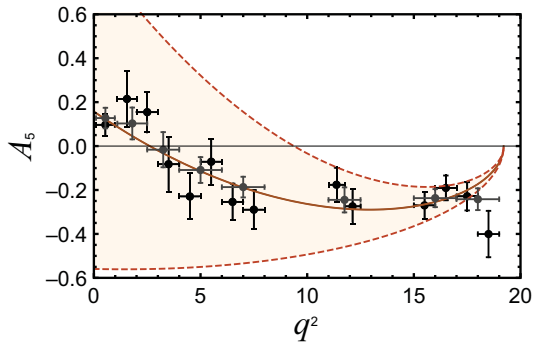

Figure 4. An analytic fit to 14-bin LHCb data using Taylor expansion around $q^2_{\rm max}$ for the asymmetry A_5 is demonstrated. The central fit function is shown as the brown curve. The light brown shaded regions denote the $\pm 1\sigma$ error bands. The LHCb 14-bin and 8-bin measurements [14] are indicated by the points with the black and gray error bars, respectively.

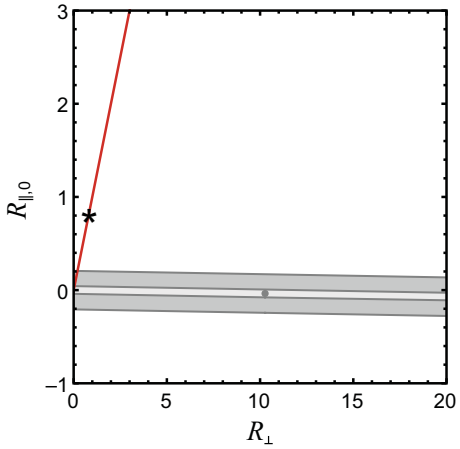

Figure 5. The allowed regions in $R_\perp$–$R_{\parallel,0}$ plane are demonstrated. The solid red straight line on the far left represents $R_\perp = R_{\parallel,0}$ with the star denoting the SM value. The gray point is the best-fit central value. The 1σ and 5σ confidence levels are denoted by the light and dark gray contours, respectively.

$A^{(1)}_{\rm FB}$ and $A^{(1)}_5$ as two independent measurements. However, we have noticed that condition for factorization, i.e. $A^{(1)}_{\rm FB} = 2A^{(1)}_5$ holds within $\pm 1\sigma$. We get $\omega_1 = 1.09 \pm 0.33$ (0.93 ± 0.36) and $\omega_2 = -2.87 \pm 6.69$ (-2.65 ± 6.18) where the first numbers and the numbers in the round brackets are obtained using the values of $A^{(1)}_{\rm FB}$ and $2A^{(1)}_5$ respectively.

3.2 *Fits on $R_\perp$–$R_{\parallel,0}$ plane*

We estimate the range of values for $R_\perp$ and $R_{\parallel,0}$ in two different ways. In the first approach, with the two obtained values of ω_1 and ω_2, we fit $R_\perp$ and $R_{\parallel,0}$ by minimizing a χ^2 function. As shown in figure 5, the light gray and dark gray contours denote the 1σ and 5σ allowed regions in the $R_\perp$–$R_{\parallel,0}$ plane with the gray dot as the central value, whereas the solid red straight line on the left corresponds to $R_\perp = R_{\parallel,0}$ case with the black star as the SM value. In SM, the contours should be aligned along the 45° straight line even in the presence of resonances as all helicities get equal contributions from resonances through ΔC_9 in eq. (2). Hence, the deviation of the contours from the SM expectation is a signal for RH currents.

In an alternative approach, we took the coefficients of observables, i.e. $F^{(1)}_{\rm L}$, $F^{(1)}_{\rm P}$, $A^{(1)}_{\rm FB}$, $A^{(1)}_5$, $A^{(2)}_{\rm FB}$ and $A^{(2)}_5$ as Gaussian distributions with central values and errors, taken from table 1, as means and standard deviations. Then $R_\perp$ and $R_{\parallel,0}$ are estimated by choosing the values of these coefficients randomly. In the absence of RH, the points indicating different values of $R_\perp$ and $R_{\parallel,0}$

should lie along a straight line with a 45° slope in the $R_\perp - R_{\parallel,0}$ plane. But we find a slope that is nearly 0°, indicating that $R_\perp \gg R_{\parallel,0}$. The deviation of slope from 45° indicates the presence of contributions from RH currents.

As discussed in ref. [7], the value of ω_1 always enhances due to charmonium resonance contributions in bin-averaged data. But we found the value of ω_1 to be close to the lowest possible physically allowed value. In a study of resonance effects in $B \to K\ell^+\ell^-$ [17], the difficulty in accommodating the LHCb-result in the standard treatment of the SM or QCD was noted and it was also suggested that contributions from right-handed current might be seen in this mode.

3.3 *Estimates of ξ and ξ'*

As the presence of RH currents are clear from the R_λ values, we want to get an estimate of the corresponding Wilson coefficients, i.e. C_9' and C_{10}'. Hence, using eqs (18), (32) and (33), we perform a χ^2 fit to ξ and ξ' with r/C_{10} as an input, estimated from eq. (26), at $q^2_{\max}$. The allowed region for ξ and ξ' values are shown in figures 6 and 7 as contours in the ξ–ξ' plane. Figure 6 demonstrates the region obtained using the SM estimated values of the parameter r/C_{10}, i.e. $r/C_{10} = 0.84$. -0.83 ± 0.82 and -0.90 ± 0.28 are the ξ and ξ' best-fit values with $\pm 1\sigma$ errors, respectively. The 1σ, 3σ and 5σ confidence level regions are denoted by yellow, orange and red bands, respectively. The star, which lies beyond the 5σ confidence level contour in figure 6, indicates the SM values of C_{10}'/C_{10} and C_9'/C_{10}. However, in figure 7 it sits just outside the 3σ confidence level contour.

However, the r/C_{10} value can change with contributions within SM, e.g. errors in the Wilson coefficients or resonance contributions, or from other kinds of NP. Hence, we have analysed the $\xi - \xi'$ values over a set of r/C_{10} values [7]. One of these samples is shown in figure 7. In figure 7, we show that the ξ and ξ' best-fit central values are reduced if r/C_{10} is smaller which could be due to NP contributions that alter the Wilson coefficient C_9. Also, the significance of discrepancy can be reduced $\sim 3\sigma$. The value $r/C_{10} = 0.6$ could be from a scenario in which the Wilson coefficient C_9 gets an additional NP contribution, i.e. $C_9^{\rm NP} \approx -1$, as shown by global fit analysis for $b \to s$ transition [2]. With this value of r/C_{10}, the ξ and ξ' best-fit values with $\pm 1\sigma$ errors are -0.87 ± 0.60 and -0.67 ± 0.27, respectively.

We note that if $\xi \neq 0$ is confirmed, then additional scalar and/or pseudoscalar contributions would be required to have consistency with $B_s \to \mu^+\mu^-$ data [18].

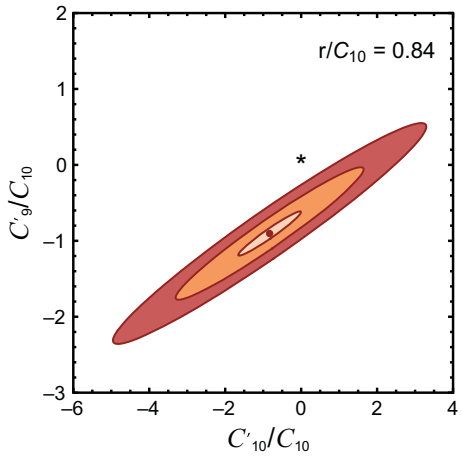

Figure 6. Allowed regions in C_{10}'/C_{10}–C_9'/C_{10} plane are demonstrated. The 1σ, 3σ and 5σ confidence level regions are denoted by yellow, orange and red bands, respectively. The red dot in the centre denotes the best-fit point. The star, which lies beyond the 5σ confidence level contour, indicates the SM values of C_{10}'/C_{10} and C_9'/C_{10}. The plots use the SM estimated value of r/C_{10}.

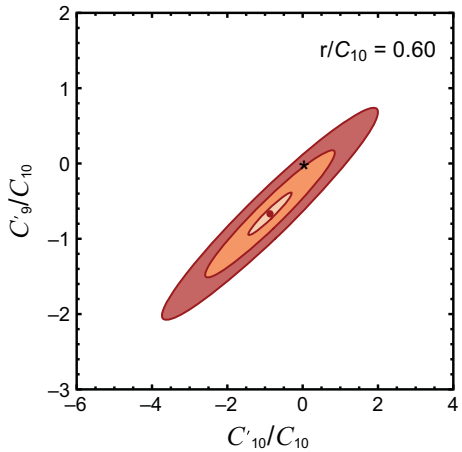

Figure 7. Allowed regions in C_{10}'/C_{10}–C_9'/C_{10} plane are demonstrated. The 1σ, 3σ and 5σ confidence level regions are denoted by yellow, orange and red bands, respectively. The red dot in the centre denotes the best-fit point. The star, which sits just outside the 3σ confidence level contour, indicates the SM values of C_{10}'/C_{10} and C_9'/C_{10}. These plots illustrate the sensitivity to r/C_{10}. The r/C_{10} value includes an additional NP contribution $C_9^{\rm NP} \approx -1$ [2] (see text for details).

3.4 *The imaginary contributions and finite K^* width*

In this section, we address the imaginary contributions to the transversity amplitudes, i.e. ε_λs from eq. (3), which has been ignored so far. We estimate ε_λs from the LHCb data. These imaginary contributions do not affect the asymmetries. However, they contribute to the helicity fractions, i.e. F_λ, as shown in [8].

We Taylor expand the quantity $\hat{\varepsilon}_\lambda \equiv 2|\varepsilon_\lambda|^2/\Gamma_f$ and use LHCb data to determine the coefficients of the expansions, i.e. $\hat{\varepsilon}_0^{(0)}$, $\hat{\varepsilon}_0^{(1)}$, $\hat{\varepsilon}_\parallel^{(1)}$ and $\hat{\varepsilon}_\perp^{(1)}$, which change the estimated values of ω_1 and ω_2. We also study the finite K^* width effects on our conclusions. The details are given in ref. [7]. We show that our results are slightly strengthened after including these effects.

4. Conclusion

We show how RH currents can be probed, at q^2_{max}, without worrying about hadronic approximations. Our approach is clean as it relies only on heavy quark symmetries where it is valid without significant corrections. This is unique in the sense that we look at the slopes of the observables at the endpoint in search of NP. This is because NP does not change the values of the observables at the endpoint (i.e. q^2_{max}), rather it changes the derivatives at the endpoint. The disparity between $R_{\parallel,0}$ and $R_\perp$ indicates the presence of RH currents. We find a 5σ evidence of NP at q^2_{max} from the LHCb data. The numbers can improve with more data around q^2_{max}. Nonetheless, we claim a clear evidence of RH currents. However, there can be other kinds of NP present in addition to the RH currents which reduce the ξ and ξ' values obtained in this work.

Acknowledgements

The authors thank Marcin Chrząszcz, Nicolla Serra and other LHCb collaboration members for comments and suggestions. The authors also thank B Grinstein, N G Deshpande and S Pakvasa for their expert opinions on the matter. T E Browder thanks US DOE for their support.

References

[1] F Kruger, L M Sehgal, N Sinha and R Sinha, *Phys. Rev. D* **61**, 114028 (2000), arXiv:hep-ph/9907386
[2] W Altmannshofer and D M Straub, *Eur. Phys. J. C* **75**(**8**), 382 (2015)
M Ciuchini *et al*, arXiv:1512.07157
S Jäger and J Martin Camalich, *Phys. Rev. D* **93**(**1**), 014028 (2016)
S Descotes-Genon, L Hofer, J Matias and J Virto, arXiv:1510.04239 and references therein
[3] B Grinstein and D Prijol, *Phys. Rev. D* **70**, 114005 (2004)
[4] C Bobeth, G Hiller and D van Dyk, *Phys. Rev. D* **87**(**3**), 034016 (2013)
[5] R Mandal and R Sinha, arXiv:1506.04535 [hep-ph]
[6] G Hiller and Roman Zwicky, *J. High Energy Phys.* **1403**, 042 (2014)
[7] A Karan, R Mandal, A K Nayak, R Sinha and T E Browder, arXiv:1603.04355 [hep-ph]
[8] R Mandal, R Sinha and D Das, *Phys. Rev. D* **90**(**9**), 096006 (2014)
[9] M Beneke, T Feldmann and D Seidel, *Nucl. Phys. B* **612**, 25 (2001), arXiv:hep-ph/0106067
[10] A Khodjamirian, T Mannel, A A Pivovarov and Y-M Wang, *J. High Energy Phys.* **1009**, 089 (2010)
[11] W Altmannshofer *et al*, *J. High Energy Phys.* **0901**, 019 (2009) , arXiv:0811.1214 [hep-ph]
[12] C Bobeth, G Hiller and D van Dyk, *J. High Energy Phys.* **1007**, 098 (2010)
[13] D Das and R Sinha, *Phys. Rev. D* **86**, 056006 (2012), arXiv:1205.1438 [hep-ph]
[14] LHCb Collaboration: R Aaij *et al*, *J. High Energy Phys.* **1602**, 104 (2016)
[15] LHCb Collaboration: R Aaij *et al*, arXiv:1606.04731 [hep-ex]
[16] F Beaujean, M Chrząszcz, N Serra and D van Dyk, *Phys. Rev. D* **91**, 114012 (2015).
[17] J Lyon and R Zwicky, arXiv:1406.0566 [hep-ph]
[18] K De Bruyn, R Fleischer, R Knegjens, P Koppenburg, M Merk, A Pellegrino and N Tuning, *Phys. Rev. Lett.* **109**, 041801 (2012), arXiv:1204.1737 [hep-ph]